AAS 15-218

SFDT-1 CAMERA POINTING AND SUN-EXPOSURE ANALYSIS AND FLIGHT PERFORMANCE

Joseph White,* Soumyo Dutta,† and Scott Striepe‡

The Supersonic Flight Dynamics Test (SFDT) vehicle was developed to advance and test technologies of NASA's Low Density Supersonic Decelerator (LDSD) Technology Demonstration Mission. The first flight test (SFDT-1) occurred on June 28, 2014. In order to optimize the usefulness of the camera data, analysis was performed to optimize parachute visibility in the camera field of view during deployment and inflation and to determine the probability of sun-exposure issues with the cameras given the vehicle heading and launch time. This paper documents the analysis, results and comparison with flight video of SFDT-1.

INTRODUCTION

The Supersonic Flight Dynamics Test (SFDT) vehicle was developed to advance and test technologies of NASA's Low Density Supersonic Decelerator (LDSD) Technology Demonstration Mission. The first flight test (SFDT-1) occurred on June 28, 2014. As part of the test, a ballute was used as a Parachute Deployment Device (PDD) to extract the main parachute, a Supersonic Disk Sail (SSDS), from the vehicle and from the bag into which it was packed. Success of the parachute depended largely on these deployment events (end of Test Period in Figure 1) that occurred over a short period of time and involved both the PDD and SSDS. To aid in analysis of these events, several cameras were mounted on a mast on the aft deck of the vehicle and pointed aft in an attempt to capture the deployment and inflation events. The problem arose to determine which pointing orientation had the highest probability of capturing those key events.

The Program to Optimize Simulated Trajectories II (POST2) simulation was used to simulate vehicle attitude and trajectory from balloon drop to splashdown and included modeling the PDD and parachute during those extraction events[1]. The test vehicle (TV), PDD pack, deployed PDD, SSDS pack, and deployed SSDS were modeled as separate, six-degree-of-freedom bodies in POST2. Flexible lines connected the PDD and SSDS to the TV to couple their dynamics. Monte Carlo analysis was used to determine performance statistics of interest for each of the bodies modeled. Modeling capability was added to POST2 to improve the tracking of the PDD and SSDS relative to the location of the cameras while accounting for the field of view (FOV) of each camera and the size of the deployed SSDS. Analysis was performed using these capabilities in POST2 to determine which camera orientation would provide the highest probability of capturing specific parachute extraction events, such as line stretch, bag strip, and inflation.

* Senior Project Engineer, Analytical Mechanics Associates, Inc, 21 Enterprise Parkway, Suite 300, Hampton, VA 23666-6413
† Aerospace Engineer, NASA Langley Research Center, 1 North Dryden St., Hampton, VA 23681-2199
‡ Aerospace Engineer, NASA Langley Research Center, 1 North Dryden St., Hampton, VA 23681-2199

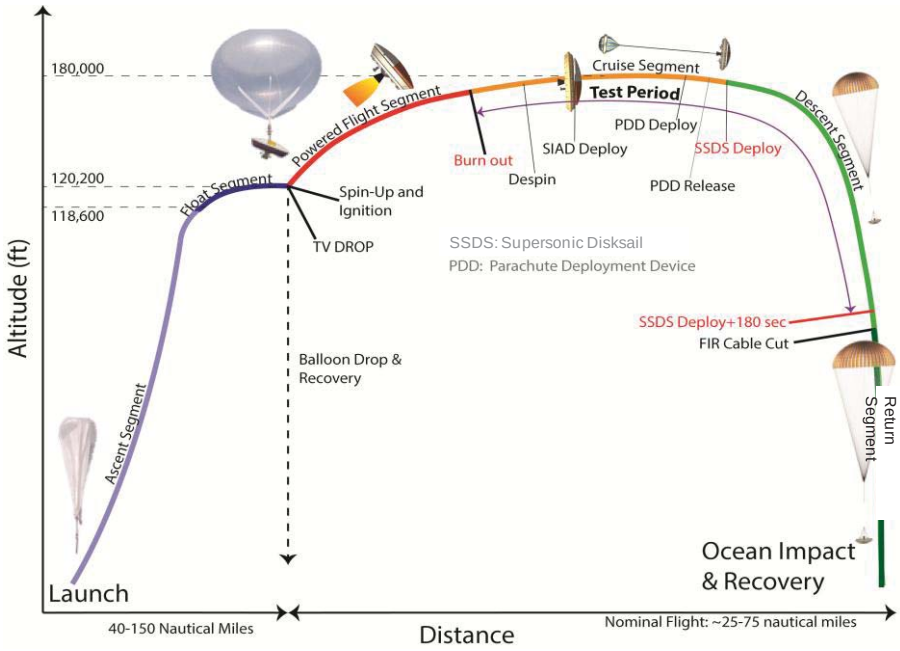

Figure 1. SFDT-1 Concept of Operations (CONOPS)

Additionally, this capability was used in analysis for the similar issue of camera sun-exposure. Given the time of day and vehicle heading at balloon drop, the sun would potentially appear for some duration of time in the cameras' FOVs during flight. With the sun inside a camera's FOV, the usefulness of returned video data would be reduced or eliminated due to over exposure of the camera sensor. With a trade space of a range of vehicle headings and drop times, a desired heading was determined which would minimize the amount of sun-exposure.

During the flight test, there was an anomaly with the SSDS which caused it to fail during inflation. However, the flight data retrieved is still useful for comparison with the results of the camera and sun-exposure analyses discussed here. This paper documents some of the details of flight related to the camera pointing study, the capabilities added to POST2 to perform the camera pointing and sun-exposure analysis, and shows that the flight results compare well with predicted performance from the analyses conducted.

DETAILS OF RELEVANT FLIGHT EVENTS

A small subset of flight events most relevant to the cameras mounted on the aft of the TV are described here. They include the deployment and inflation of the PDD and SSDS. The primary purpose of the cameras was to capture those events and the dynamic response of the TV would impact how well the PDD and SSDS deployments were captured by the cameras.

One of the primary goals of SFDT-1 was to test a supersonic inflatable aerodynamic accelerator (SIAD). This portion of the flight is noted in Figure 1as the test period. Its purpose is to reduce the velocity of the TV to conditions more suitable for the deployment of the SSDS.

Towards the end of the SIAD test period, the PDD deployment was triggered either by a velocity condition or a no-later-than timer. When the deployment was triggered, a mortar fired to deploy the PDD pack from the TV. This mortar fire not only deployed the PDD pack, but also imparted a significant reaction force on the TV, inducing some oscillations in the angle of attack. When the

PDD reached line stretch, an inflation aid device quickly inflated the body, increasing its drag and pull on the TV.

The end of the SIAD test period was approximately five seconds after PDD deployment was been triggered. At this time, the triple bridle restraining the PDD was cut, leaving only a line attached to the SSDS pack from the PDD. The drag from the PDD provides the force to extract the SSDS pack from the TV. During extraction, the friction between the SSDS pack and the TV allowed some of the drag of the PDD to pull on the TV which increased its angle-of-attack oscillation. Once line stretch was reached, the SSDS bag pulled away with the PDD, extracting the canopy and starting the inflation process. Once the SSDS was inflated, the vehicle dynamics approached steady state conditions.

Given the dynamics induced by these events, the problem became one of optimizing the pointing orientation of the cameras to maximize the probability of capturing the events of interest. Additional capability was needed to determine when the various bodies were in the FOV of each camera, both when stowed in packs during deployment and while inflated. Including this capability in the Monte Carlo analysis used with the simulation provided the information needed to determine the optimum orientation.

POST2 CAPABILITIES

POST2[2] is a trajectory simulation program with multi-body capabilities that integrates translational and rotational equations of motion along the trajectory. To better understand the additional capability added to POST2 to address the camera analyses, a background on other current capabilities will be briefly given. These capabilities include multiple body modeling, SPICE ephemeris integration, and the antenna subsystem used for tracking objects. Finally, the added capability for FOV calculations and its use will be described.

Multi-Body and SPICE

In the POST2 simulation, the TV, SSDS, SSDS pack, PDD, and PDD pack were each modeled as separate, six degree of freedom bodies. Flexible lines were modeled as needed between bodies and created constraint forces between them. Position, velocity, attitude, and attitude rate were tracked for each body independently. This multi-body capability allows POST2 to track the state of one body relative to another.

Similar to the multi-vehicle capability, tracking of the sun was needed to perform the sun-exposure analysis. Integration of the SPICE ephemeris database into POST2 allowed for the relative state calculation between the sun (and other celestial bodies) and the spacecraft.

Antenna Subsystem

Both the multi-vehicle and SPICE capabilities were essential for the camera studies described here. However, they were limited to calculating relative states between the centers of gravity of the bodies of interest. To aid in multi-body interaction and understanding, the antenna subsystem in POST2 can be used to track other vehicles and targets. An antenna is considered to be a frame-fixed tracking system for relative state data. The antenna tracks a user-defined marker placed at any location on a specified body (e.g. vent location at the center of the parachute). A boresight vector is defined in a frame of choice and used as a reference for relative state calculations. Figure 2 gives a graphical representation of the antenna frame and some of the relative states calculated in this manner.

Figure 2. Graphical Description of the Antenna Subsystem[2]

For example, an antenna could be defined on the TV at the location of the cameras with its frame aligned with the TV body frame and its boresight aligned with the camera line of sight. The target could be configured as either the sun or marker on other body of interest. Markers on the target allow for the antenna to track a specific location on the target and not just the center of gravity. Setup in this way, relative state data will be calculated between the camera's line of sight and the target vehicle or body.

POST2 was able to perform these relative state calculations using the antenna subsystem, multi-body and SPICE capabilities at every integration time step of the simulation. Tracking those values and their extremes provided much of the data of interest. The one remaining capability required for the camera analysis was the FOV calculations to determine when the target was bounded within a specified view.

Field of View Determination

The addition of FOV calculations was necessary to complete the analyses for the camera pointing and sun-exposure. FOV is defined either by a single angle for a circular FOV (black dashed circle on left) or by high, low, vertical, and horizontal angles that define a rectangular or square (green dashed square on right) FOV as shown in Figure 3 below. For the SFDT-1 camera analyses, the FOV was specified as rectangular using the manufacturer specifications for each camera.

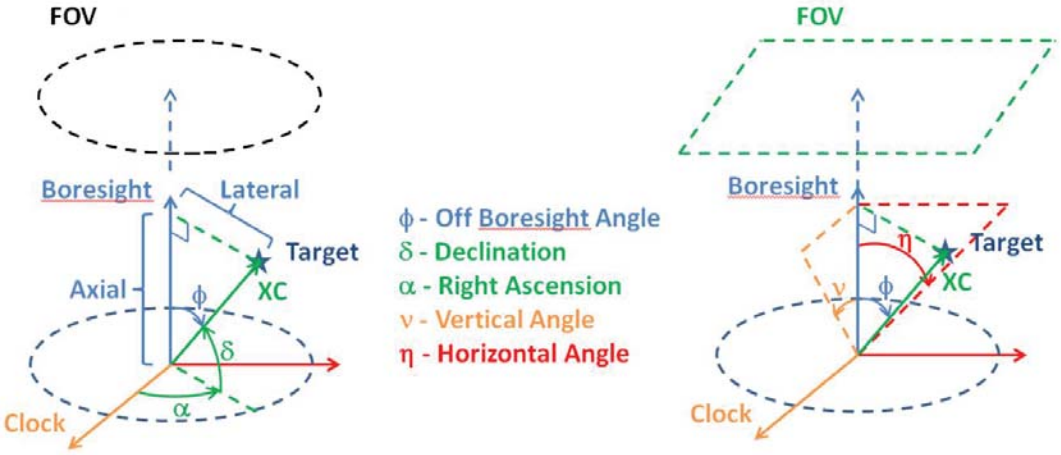

Figure 3. Antenna Subsystem Description with the Field of View Addition

At each time step, the location of the target was determined relative to the antenna (and its boresight) and a flag was set to indicate whether the target was within the antenna's FOV or not. For circular FOVs, the off-boresight angle could be used to quickly make the determination. For rectangular FOVs, the horizontal and vertical angles were compared with the FOV.

An additional capability added to POST2 is that of multiple FOV layers per antenna. For the camera pointing analyses in particular, the benefit of a layered FOV was the ability to track both the vent of the SSDS (a point) and the fully inflated SSDS (larger body geometry resulting in reduced effective FOV). This capability also allowed for comparing results from different lens options for a camera, as lenses of different focal lengths will have different FOVs. The implementation of this capability for the camera analyses will be described in later sections.

The visibility of the vehicles of interest to the cameras was tracked over time. In the Monte Carlo analysis, results were given for multiple discrete events. Additionally, the visibility flags were tracked over periods of time to determine if the vehicle was visible continually over a period of time or if it slips outside the FOV. With this capability in place, the optimum pointing angle for the cameras and sun-exposure risk could adequately be analyzed.

CAMERA POINTING ANALYSIS

Three cameras were mounted to a mast on the aft side of the TV with the primary intent of capturing the behavior of the SSDS as it was extracted and inflated. The three cameras each served specific purposes. A GoPro camera with the largest FOV captured the broad scene of events. A high resolution SXC-80 was capable of capturing more detail of the bodies. Finally, a Cinegon high speed camera was used to better capture the body dynamics. The three cameras were all mounted to the same mast and oriented together through an adjustable head as shown in Figure 4. The GoPro had its "up" vector oriented to be in a portrait orientation to match the alignment of the other two cameras.

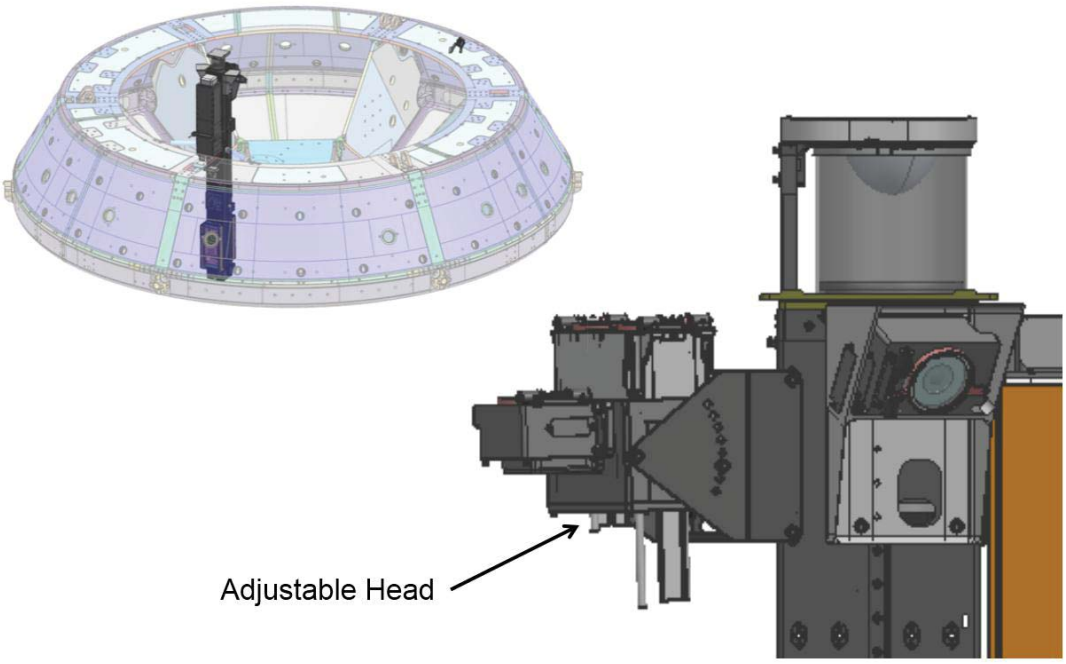

Figure 4. Model of the Camera Mast on the Aft Deck of the Test Vehicle

While directing the cameras directly aft of the test vehicle could capture the events of interest in many cases, the offset location of the cameras and the offset dynamics of the PDD mortar and SSDS pack extraction force made that orientation less likely to capture all of the events of interest.

The adjustable head used to mount the cameras has adjustments in one-degree increments from a -2 degrees to +10 degrees. Using POST2 with the tools described previously, a sweep was performed through these pointing options. For each option, an 8000 case Monte Carlo was run with line stretch and full inflation tracked for visibility. The probability of capturing both the SSDS vent and the inflated SSDS were tracked for each camera.

Table 1. Description of Cameras Mounted on Aft Mast for SFDT-1

CAMERA	DESCRIPTION	FIELD OF VIEW	
		HORIZONTAL (DEGREES)	VERTICAL (DEGREES)
GoPro	SITUATIONAL, SSRS	68	121
Cinegon	HIGH SPEED, SSRS	56.9	56.9
SXC-80	HIGH RES, SSRS	48.8	37.6

The cameras used and their corresponding FOVs from manufacturer specifications are shown in Table 1. . The rectangular FOVs were setup in POST2 using this data to track the vent of the SSDS. To track the inflated SSDS, an effective FOV for the target marker (canopy vent) was determined as follows: The reduced FOV is the range the target marker can travel while maintaining all points of the SSDS inside the full FOV (see Figure 5). The effective range is approximated by subtracting the angular coverage of the SSDS (α) from the full FOV. This was an approximation due to the fact that the cameras were not located at the pivot point of the SSDS, but provided

adequate results because of the relatively small offset of the cameras compared to the distance from the cameras to their target. Each of the three cameras used a full FOV layer, as well as an effective FOV, in this manner for tracking both the vent and the fully inflated SSDS.

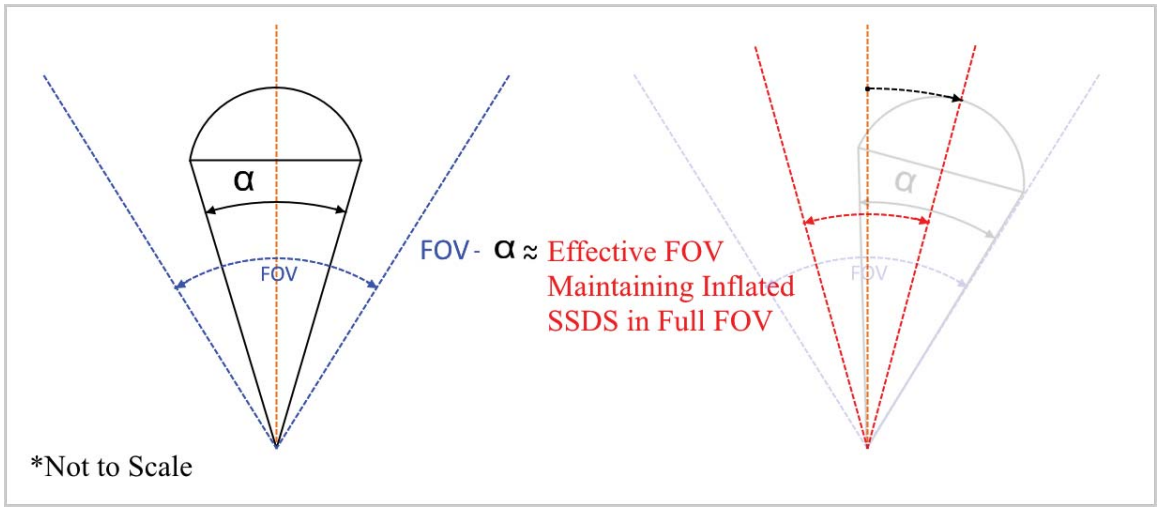

Figure 5. Effective FOV Determination for Tracking Inflated SSDS.

In the Monte Carlo analysis, visibility at both discrete events and over specific periods of time were tracked. The discrete events determine if the target was visible to a camera at a single point in time. The tracked periods were used to determine if the target was visible at all times over a specified range. If visibility was not positive for all times in over a range, then the period was flagged as not visible. Visibility criteria for both vent and full SSDS tracking are depicted in Figure 6 and Figure 7.

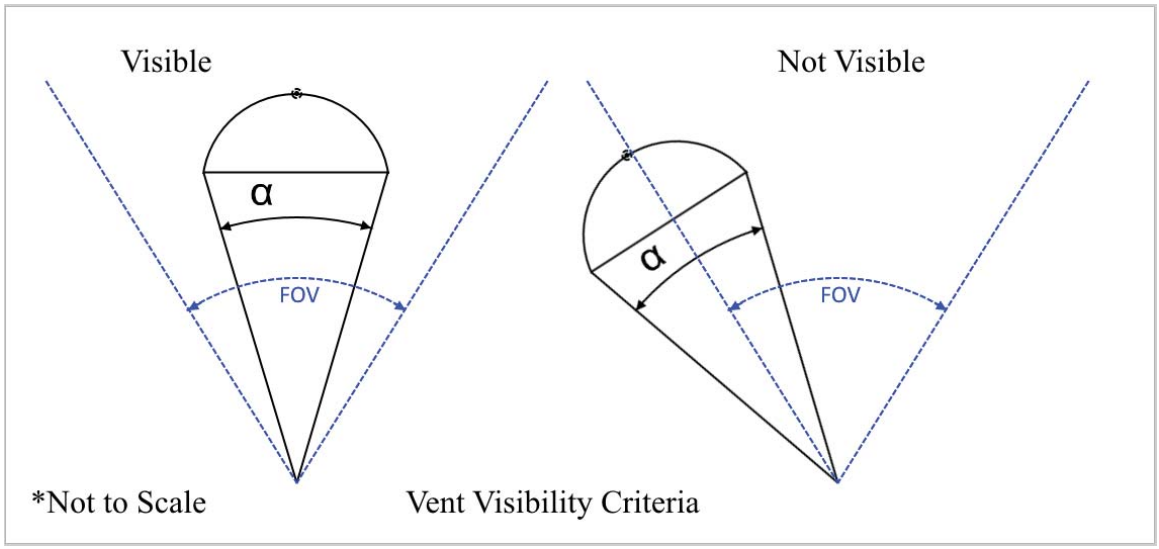

Figure 6. The Vent is Visible if the Target Marker Remains Inside the Full FOV

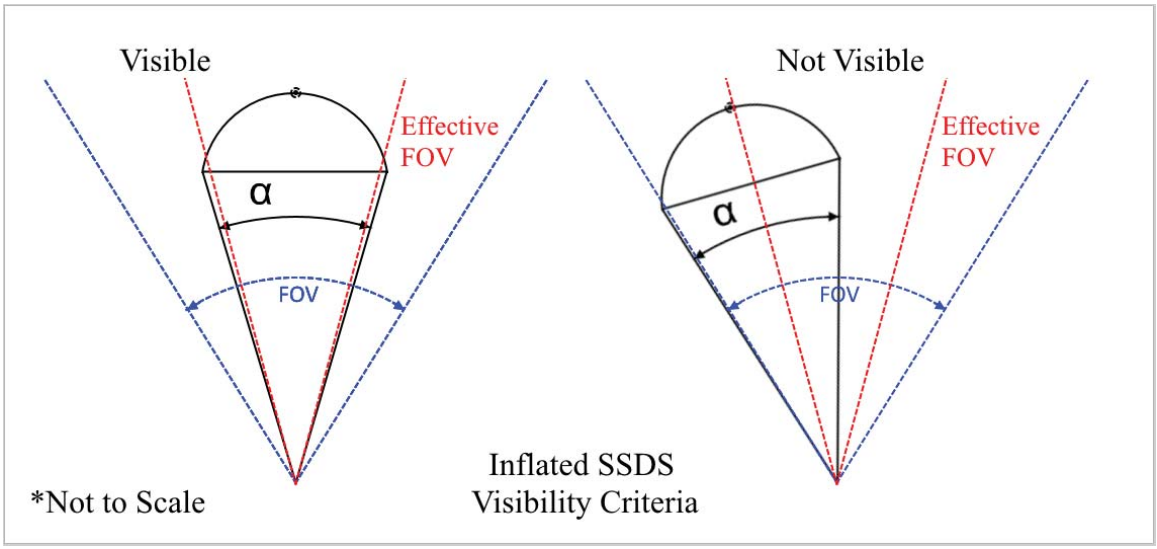

Figure 7. The Inflated SSDS is Visible if the Target Marker Remains Inside the Effective FOV

After processing the Monte Carlo runs and collecting the data, the probability of visibility was plotted for each event and camera. The results can be seen in Figure 8 for the line stretch and inflation related events. The visibility probability for the vent at full inflation (green series) shows no case that falls outside of the FOV of any of the cameras. In the figure, the green series is hidden by the data for the SSDS at full inflation (red series) which also maintains high probability (>98%) for all cameras over the full range of pointing angles.

Both the SSDS at line stretch (blue series) and the vent tracked from line stretch through full inflation (cyan series) show increasing probabilities with increasing pointing angle. Because the period tracked from line stretch through full inflation contains the line stretch event, any cases not visible at line stretch would also be counted not visible through full inflation. Thus the similar trends between the two series. The small differences in these two series indicate that only a small number of cases visible at line stretch slip outside the FOV at some other time between line stretch and full inflation.

The results of most interest here can be seen between 8 and 10-degree pointing angles. There is an intersection of the data curves for the high speed and high resolution cameras for the events of interest. This data was used to conclude that a 9-degree pointing angle maximizes the visibility probability at line stretch while minimizing the visibility fallout of the high resolution camera for the SSDS at full inflation.

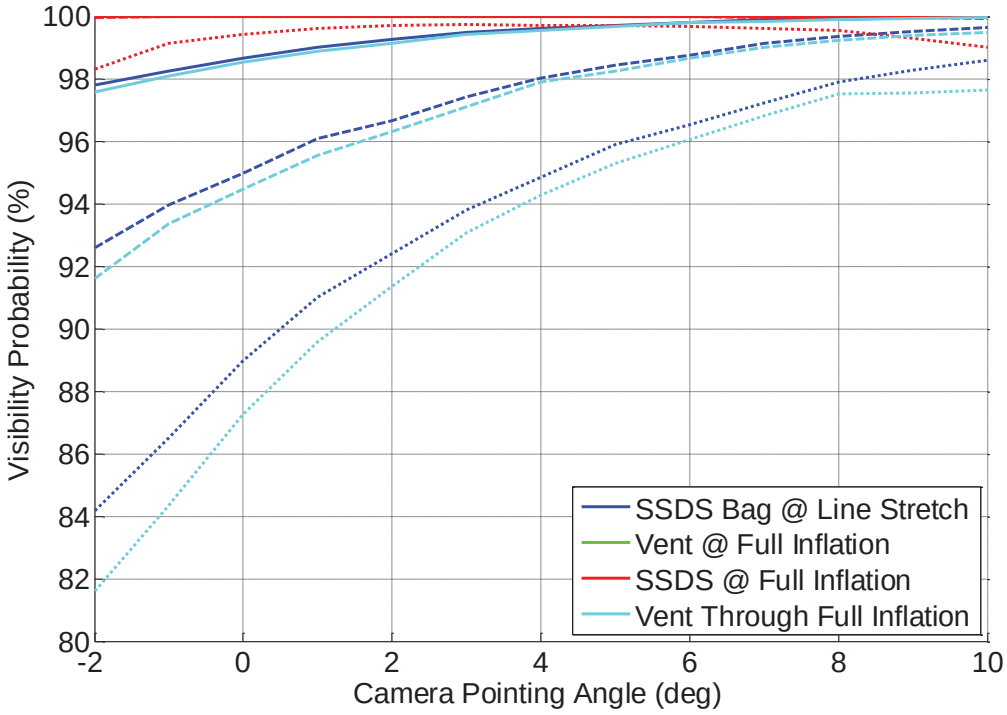

Figure 8. Visibility Probability for Line Stretch and Inflation Related Events. Solid Lines are for the GoPro, Dashed for the High Speed, and Dotted for the High Resolution.

Figure 9 shows a screen capture of all cameras at the approximate line stretch event from the SFDT-1 camera data. All cameras captured the event successfully. Because of the anomaly with the SSDS on SFDT-1, a full inflation event was not well defined. A screen capture from each of the cameras was taken at the approximate first instance of the SSDS showing full diameter. This approximate event was also captured successfully and the screen captures are shown in Figure 10. The analysis discussed here was not tracking an actual location of the target within the camera FOV, but simply flagging as visible or not visible. Because of this, the analysis described here was not used to specifically determine any level of off-nominal behavior in SFDT-1.

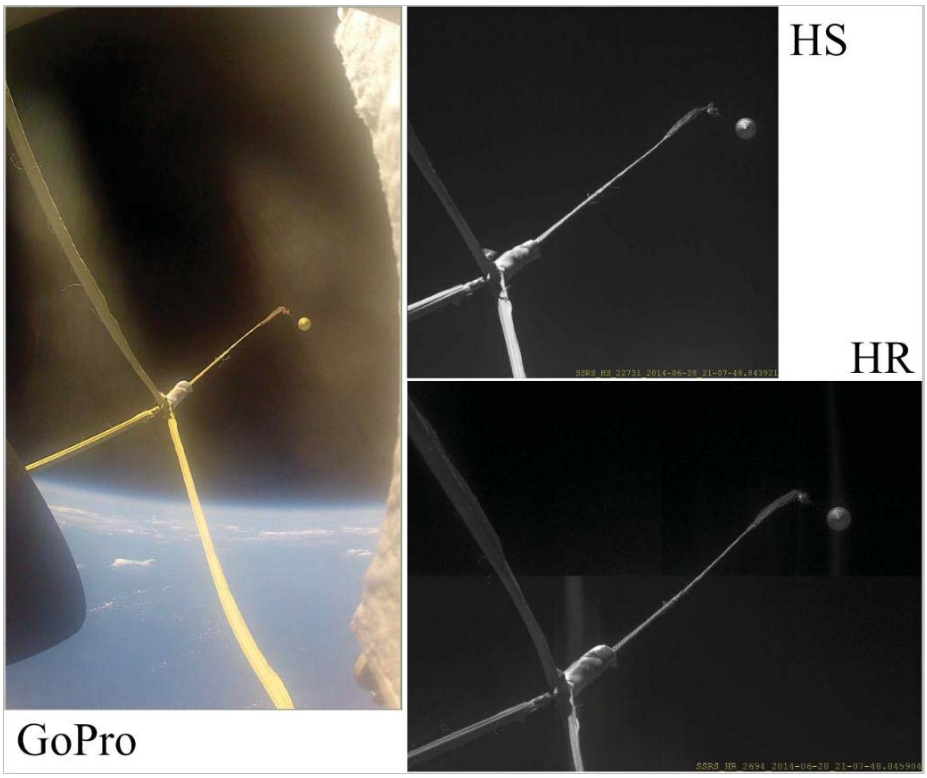

Figure 9. Screen Capture from Cameras at Approximate Line Stretch Event.

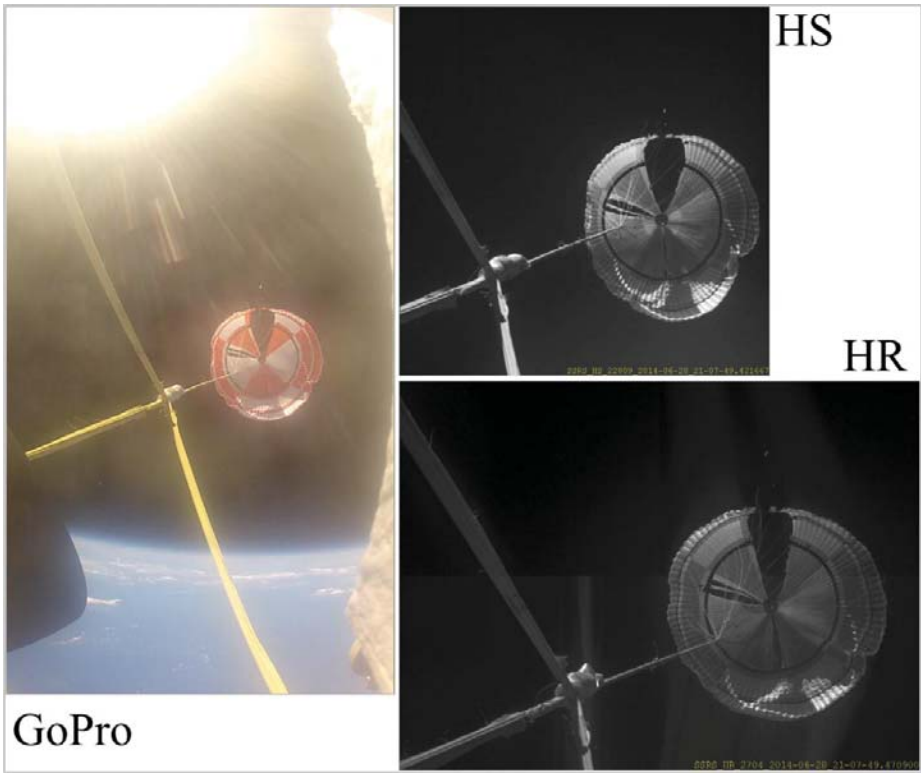

Figure 10. Screen Capture from Cameras at Approximate Full Inflation Event.

SUN EXPOSURE ANALYSIS

The cameras on SFDT1 were set at constant brightness and contrast settings. Thus, exposure to the sun would greatly reduce the usefulness of the returned video data, as can be seen in a frame from SFDT1 in Figure 11. Fortunately, the initial heading angle of the test vehicle dictated the amount of sun exposure seen by the three main cameras and this angle was a control that could be chosen before test vehicle drop from the balloon. The main concern with the heading angle was range safety so that the vehicle splashdown occurred in a safe zone. However, limiting the sun exposure to the camera became an important second priority in choosing the heading angle since the video data from SFDT1 was one of the most valuable measurements from the mission. The multi-body dynamics and camera pointing mechanism in POST2 that was described in previous sections were also used to determine how to lessen the camera's exposure to the sun.

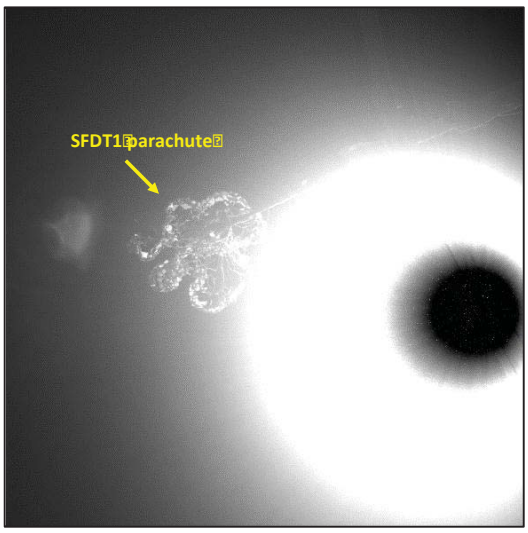

Figure 11. Still Frame from the SFDT1 High-Speed Camera with the Sun in the Field of View.

Similar to previous discussion, the cameras considered for the sun exposure analyses were the three up-look cameras, namely, the situational GoPro, high-resolution SXC-80, and high-speed Cinegon. Also similar to previous sections, the boresight vector, the field of view dimensions, and the location of the cameras on the test vehicle determined what was seen through the camera at any point. In the last section, the targets of the camera were the PDD or the supersonic parachute that were tracked over the trajectory of the main vehicle. For the sun exposure study, the sun was an additional object that was tracked. The sun ephemeris was provided by SPICE kernels released by the NASA Navigation and Ancillary Information Facility and the sun was modeled as a circle with angular diameter that stayed constant with altitude. The geometry model used for the sun exposure study is further described in Figure 12.

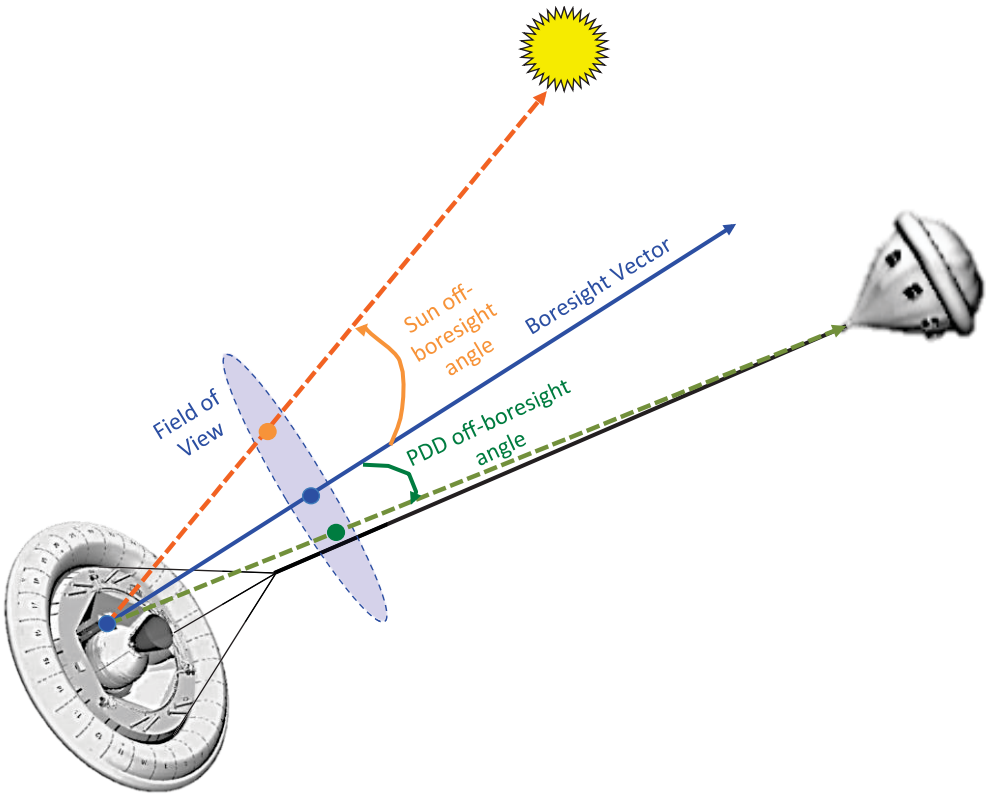

Figure 12. Notional Description of the Geometry Involved in the Sun Exposure and Camera Pointing Analyses. Note That the Bodies Are Not to Scale.

The two independent variables in the sun exposure study were the heading angle of the vehicle at drop from the balloon and the time of the day. The analysis was done for the first test opportunity initially scheduled for June 3, 2014 (although it finally took place on June 28, 2014) where balloon drop was timed to take place close to 10 AM local time in a 56 deg. heading angle. However, there was a possibility that the drop could take place at any point up to 2 PM local time and the heading angle was unrestricted as long as range safety was not compromised.

Thus, Monte Carlo analyses were conducted where various trajectory and environmental parameters were varied for various combinations of initial drop time and heading angles to aggregate statistics to inform the flight team of the sun exposure risks. Since all three up-look cameras had the same boresight vector (although each camera had different field of view dimensions and were mounted in different places on the vehicle), they all had very similar histories of off-boresight vector angles to the sun. Figure 13 shows the minimum sun angles (or off-boresight vector angles) observed during the Monte Carlo trajectories and tallies the 1st and 10th percentile statistic.

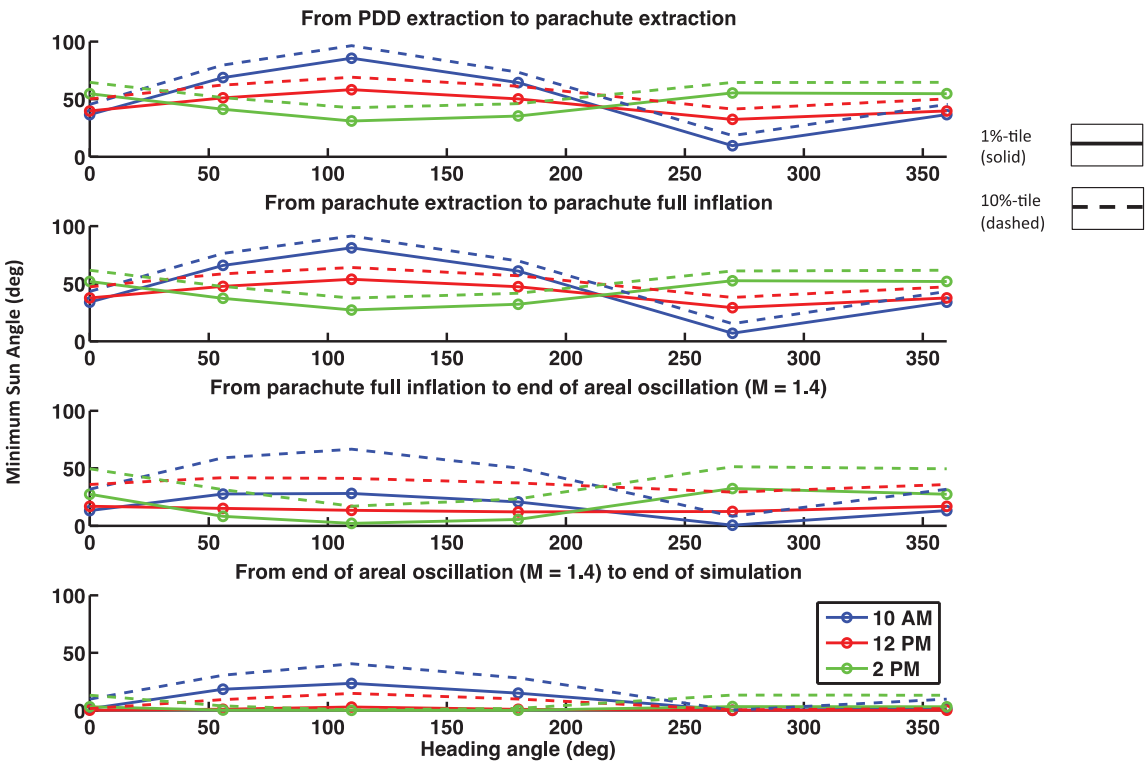

Figure 13. Sun Off-Boresight Angles for the Three Up-Look Cameras.

A small sun angle means the sun is closer to the boresight vector of the camera and hence the sun exposure risk is highest. It can be seen from the Figure 13 that the least amount of sun exposure (largest minimum sun angle) was during 10 AM and 12 PM at 110 deg. heading angle, although heading angles of 56 and 180 deg. were only slightly less desirable. The 2 PM drop had the best sun angles at 270 deg. heading but, for that time window, all heading angles had generally worse sun exposure statistics than earlier times. Additionally, note that the sun exposure statistics worsened as one moved further along the trajectory as the flight path angle steepened. From PDD extraction to parachute extraction, the sun angle remained large, but as the vehicle remained on the parachute longer, the sun came into the view of the camera until the sun angles were close to zero.

In addition to the minimum sun angle, it was important to note how many times the sun entered the camera field of view and what percentage of the recording time the sun stayed in the field of view. As mentioned before, the brightness and contrast settings for the camera were set as constants. Therefore, the number of times the sun entered the field of view was congruent to how many times the view could be completely saturated. The cameras had some latency time, so that a high frequency of sun appearances would significantly reduce the quality of the data. Figure 14 shows the 90th and 99th percentile statistics for the number of times the sun appeared in the camera field of view. Due to the similarity in the field of view size with the high speed and high resolution cameras, only one set of statistics are shown to avoid redundancy.

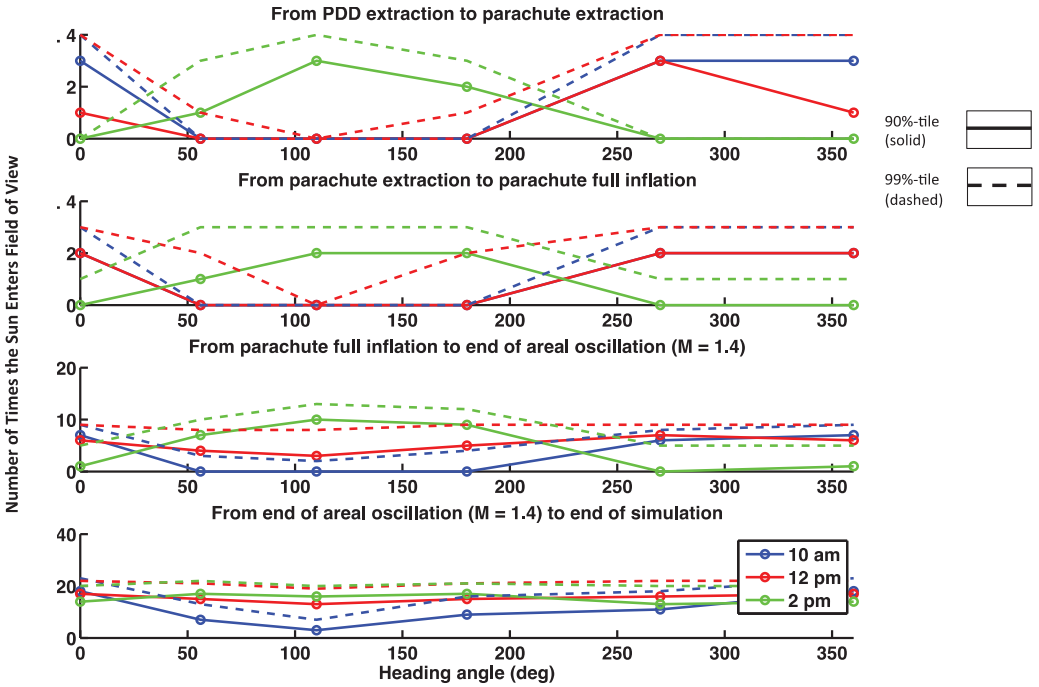

(a) Camera 4 – Up-look situational camera (GoPro)

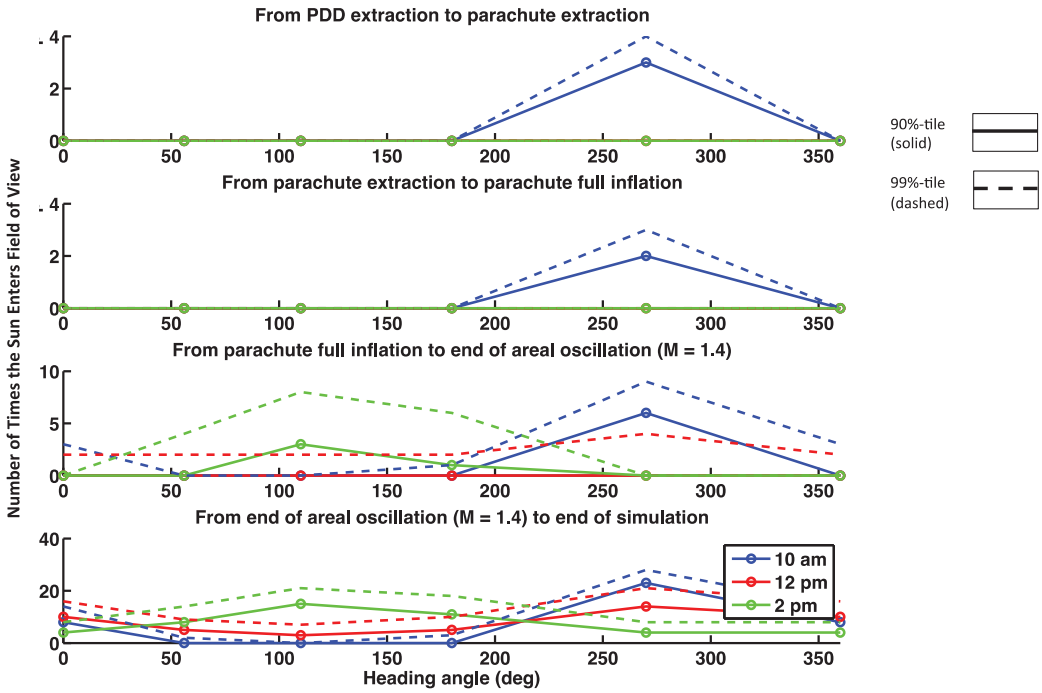

(b) Camera 7 – High-resolution camera (SXC-80)

Figure 14. Number of Sun Exposures in Two of the Three Up-Look Cameras as a Function of Heading Angle and Drop Time.

An interesting observation can be made by comparing Figure 13 and Figure 14. All three cameras had the same boresight vector and, although they were located at different parts of the vehicle, they had close to identical sun angles. However, the three cameras did have different FOV sizes, with the situational camera having the largest FOV and the other two being smaller but similar size to each other. So, by observing from Figure 14 that the number of times the sun comes into the FOV is high for the situational camera and lower for the high-speed and high-resolution camera, it can be postulated that when the sun came into the situational camera it was on the outer limb of the FOV. Although this observation was initially made from Monte Carlo analysis statistics it was later verified with individual run cases.

The actual percentage of time the sun was in the camera FOV is compared with pre-flight predictions in Table 2. The actual heading angle during the flight was 54 deg. due to a balance between range safety and sun exposure, but the 56 deg. heading angle predictions are shown in the table. Additionally, the actual flight occurred around 11 AM local time, so the 10 AM and 12 PM predictions are both shown for comparison. Table 2 is broken up into various flight phases. The data for flight segments after parachute deployment (SSDS deploy) are not shown since the parachute developed large tears in the fabric leading to off-nominal behavior that were not modeled when the predicted values were generated.

Table 2. Percentage of Time Sun is in FOV of Camera with 56 Deg. Heading Angle at Drop (99 percentile Prediction vs. Actual).

Flight Phase	Situational GoPro			High-Speed (Cinegon)			High-Resolution (SXC-80)		
	10:00 Prediction	12:00 Prediction	Actual	10:00 Prediction	12:00 Prediction	Actual	10:00 Prediction	12:00 Prediction	Actual
PDD extraction to SSDS extraction	0	6.72	24	0	0	0	0	0	0
SSDS extraction to SSDS deploy	0	22.09	45	0	0	0	0	0	0
SSDS deploy to end of areal oscillation	9.31	38.16	N/A	2.02	7.6	N/A	0	3.9062	N/A
End of areal oscillation to end of simulation	41.86	83.55	N/A	8.72	40.37	N/A	2.94	27.01	N/A

From Table 2, it can be seen that the situational camera was predicted to have the sun in the FOV a significantly larger percentage of the time than the high-speed and high-resolution cameras. Moreover, predictions for the 10 AM drop time had a smaller percentage of time with sun in the FOV than 12 PM. The actual sun exposure statistics gleaned from flight data shows that the high-speed and high-resolution cameras did not have any sun exposure during the flight segments from PDD extraction to parachute full deploy, similar to what was predicted. However, the sun exposure was higher for the situational camera for those two flight phases than what was predicted. The higher sun exposure statistics can be explained by the steeper than nominal flight path angles for PDD and parachute deploy events for the actual flight. More importantly, the sun exposure did not obscure the flight articles and the sun was only seen in the outer limbs of the camera as seen a screen still in Figure 15, confirming that particular pre-flight observation.

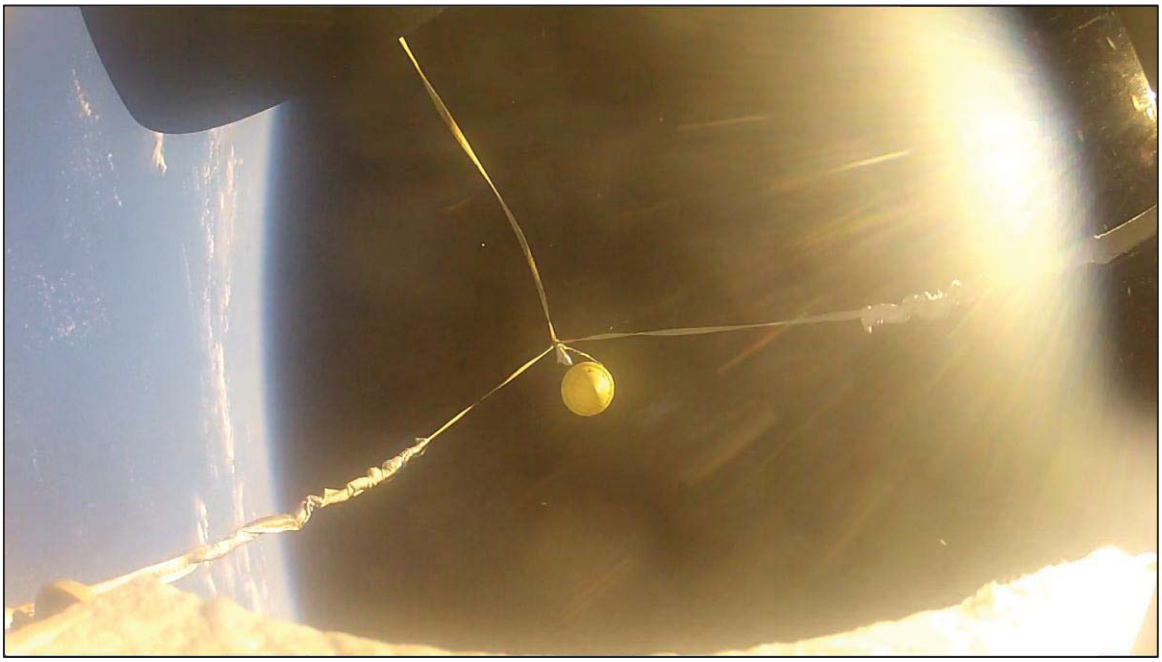

Figure 15. Sun Seen in the Outer Limb of the FOV of the Situational GoPro Camera during the Phase from PDD Extraction to SSDS Extraction.

CONCLUSION

Significant effort went into the design of the SFDT-1 test vehicle to ensure maximum amount of useful data returned. Part of the returned data is the flight video from multiple cameras on board the vehicle. Several design problems were addressed in order to maximize the usefulness of the returned camera data.

Two problems of interest were addressed by the analyses discussed here: what pointing angle to use for camera orientation and what heading angles would minimize the detrimental sun-exposure to the cameras. Relevant flight events and problems associated with the camera pointing analysis have been described. a. The new FOV capability added to POST2 has been detailed in its design and use as well as the existing capabilities that it built upon. Substantial amounts of data were generated to produce statistical results used to determine the optimum camera pointing angle needed to capture the SSDS line stretch and inflation events.

The sun-exposure problem has also been described in detail. The heading angle at balloon drop has a significant impact on the amount of sun-exposure to which the cameras are subjected. Using the same FOV calculations added to POST2 for the camera pointing analysis, cases were run to provide minimum sun angles, number of sun-exposures, and percentage of time the cameras were exposed to the sun. From these results, preferred heading angles at drop for various launch times were determined.

Results from both analyses described in this paper were used in the design and operational phases of SFDT-1. The camera data returned from flight show the selected camera pointing angle successfully captured the line stretch and inflation events in all three cameras' FOVs. The sun-exposure predictions compared well with observations in flight, with the only discrepancies due to the steeper flight path angle that occurred in the off-nominal flight of SFDT-1. The additional

capability added to POST2 to perform these analyses will continue to be used for future flights to aid in similar analyses.

REFERENCES

[1] A.L. Bowes, J.L. Davis, S. Dutta, S.A. Striepe, M.C. Ivanov, R.W. Powell, and J.P. White, "LDSD POST2 Simulation and SFDT-1 Pre-flight Launch Operations Analyses," *AAS/AIAA Space Flight Mechanics Conference*, Williamsburg, VA, 2015

[2] S. A. Striepe, R. W. Powell, P. N. Desai, E. M. Queen, D. W. Way, J. L. Prince, A. M. Cianciolo, J. L. Davis, D. K. Litton, R. M. Maddock, J. D. Shidner, R. G. Winski, S. A. O'Keefe, A. G. Bowes, J. T. Aguirre, C. A. Garrison, J. A. Hoffman, A. D. Olds, S. Dutta, C. H. Zumwalt, J. P. White, G. L. Brauer, S. M. Marsh, "Program To Optimize Simulated Trajectories II (POST2): Utilization Manual," Vol. II, Version 3.0.NESC, 2014